



PRediction Of Geospace Radiation Environment and Solar wind parameterS

Work Package 4

Development of new statistical wave models
and new parametrisation and re-evaluation
of the quasilinear diffusion coefficients.

Deliverable 4.1

Report on data availability and list of chosen
locations for each wave emission.

V. Krasnosselskikh, Y. Shprits, S. Walker, and M. Balikhin

February 29, 2016

This project has received funding from the *European Unions Horizon 2020 research and
innovation programme* under grant agreement No 637302.



Document Change Record

Issue	Date	Author	Details
1.0	01/02/2015	VK/MAB/SNW	Initial draft
2.0	20/02/2015	MAB/SNW	Tidy and correct language
3.0	25/02/2015	VK/MAB/SNW	Add THEMIS

Contents

1	Introduction	3
2	Brief overview of D4.1 with respect to the overall WP4 activity	4
3	Description of data to be used in the WP4	7
4	Statistical occurrence of chorus, hiss and EMW emissions	9
4.1	Distribution of lower band chorus	9
4.2	Distribution of Hiss	14
4.3	Distribution of Equatorial Magnetosonic Waves (EMW)	15
5	Chosen locations for Chorus, Hiss and EMW emissions	15
5.1	Chorus	17
5.2	Hiss	20
5.3	Equatorial Magnetosonic Waves	23
6	Conclusion	24
7	Future work that utilises the results described in the deliverable 4.1.	26
A	The Error Reduction Ratio methodology	31

Summary

The present deliverable investigates the spatial distribution of observations of chorus, hiss, and equatorial magnetosonic waves from the satellites Cluster 4 and THEMIS A. By using a conservative scaling algorithm these spatial distributions are used to estimate the number of independent satellite tracks as functions of magnetic local time and L-shell. A set of spatial bins, covering different ranges of MLT and L-shell, are defined such that they contain sufficient points to enable a successful Error Reduction Ratio analysis to be performed later in the work package. These lists are given in the results section of this report.

1 Introduction

Currently, first principles based approaches to the forecast of the radiation belts employ numerical codes that involve solutions of the diffusion equations. VERB, a code that will be used extensively within PROGRESS, is one such example. These codes require the calculation of tensors of quasilinear diffusion coefficients to characterise the processes of particle pitch angle and energy diffusion due to their interaction with various plasma wave modes. Statistical wave models, based on spacecraft observations are required to accurately evaluate these tensor diffusion coefficients. The overall aim of WP4 is to revise the current methodology used to develop these wave models in order to generate more realistic models that better account for the dynamical processes in the radiation belts, which will potentially lead to more reliable forecasts from first principles based tools. Deliverable D4.1 is aimed at investigating the data availability, resulting in a list of chosen locations for each of the wave emissions Chorus, Hiss and Equatorial Magnetosonic Waves. These locations will be used within later tasks to study the possible improvements to wave models resulting from taking into account not only the current state of the magnetosphere but also its preceding evolution, and the dependence of waves upon the solar wind parameters.

2 Brief overview of D4.1 with respect to the overall WP4 activity

WP4 is devoted to the investigation of the occurrence of three types of waves: Chorus, Plasmaspheric Hiss and Equatorial Magnetosonic Waves (EMW) and their dependence (if any) on the solar wind characteristics. At present, models for these wave modes are organised by current geomagnetic indices (Kp or AE) (*Horne et al.*, 2013; *Meredith et al.*, 2012; *Agapitov et al.*, 2013)]. This organisation assumes that wave occurrence depends only upon current state of the magnetosphere and is independent of the evolution of the magnetosphere. Taking an extreme example this statement implies that the level of lets say chorus waves recorded when the current level of Kp is 9 (maximum value) is the same for cases when Kp was 9 for the last 12 hours or Kp = 0 (minimum value for Kp) over the same period of time. While it is possible that such an assumption is correct and the occurrence of waves does not depend on previous states of the magnetosphere, it is still unproven. One of the particular aims of WP 4 is to investigate this assumption and, if invalid, to develop an organisation for wave models that accounts for not only for the current state of the magnetosphere but also for the effect of its preceding evolution on the occurrence of chorus, hiss and EMW. The other task of WP 4 is to assess whether the organisation of wave models based on solar wind parameters as well as geomagnetic indices will better account for the variability of wave occurrence in the magnetosphere. This will be done exploiting the concept of the Error Reduction Ratio (ERR) methodology developed in the field of Systems Science (*Billings et al.*, 1989). For linear systems the correlation function is used to assess the possiblity causal relationships between measured parameters. However, application of the correlation function to a nonlinear system can produce misleading results. As an example consider a simple system with a quadratic relationship between the input to the nonlinear system X and the output Y : $Y = X^2$. If the distribution of X depends only upon the magnitude but not upon the sign, (i.e. it is symmetric with respect to positive/negative values), the estimated correlation between

Y and X will be close to zero, in spite of the fact that X is a real input into the system. The Error Reduction Ratio methodology is a generalisation of correlation analysis that may be applied to nonlinear systems. A brief description of the ERR concept is given in Appendix 1. Application of the ERR approach requires significant amounts of data. USFD has extensive experience in applying the ERR methodology, that constitutes part of the NARMAX approach, to variety of complex systems ranging from the magnetosphere, climate, human brains, and stem cells to name but a few. Previous experience, gained by the USFD group, has shown that the reliable application of this methodology requires data from 1000 or at least 800-900) independent observations (measurements). The presently available wave models represent the "global" dependence of the wave amplitude/occurrence on the current state of the magnetosphere as expressed by the geomagnetic index (AE or Kp) (e.g. *Meredith et al.*, 2012; *Agapitov et al.*, 2013). Models that account for the previous magnetospheric evolution or effects of the solar wind parameters should be "local" in the sense that the dependence of the wave occurrence in different locations may not necessary be the same. Therefore the whole equatorial cross-section of the inner magnetosphere should be divided into a number of sub-regions. The main requirement for each subregion is that it should be large enough to ensure a sufficient number of spacecraft passes that represent independent measurements a particular type of emission in order to enable a successful ERR analysis. However, as the region size increases, the accuracy of a single dependence of the wave occurrence for the whole region will decrease. To overcome these contradictory requirements variable sizes of these regions are used. In regions with a high occurrence of high amplitude waves of a particular type chosen regions size may be smaller in comparison to other regions with a lower occurrence of these waves. One of the justifications for this approach is that regions with a high occurrence of high amplitude waves produce the most significant effect on the electron pitch angle and energy diffusion.

The wave amplitude distributions have well pronounced non-Gaussian characteristics. The tails of these distributions, which correspond to large amplitude waves, are very

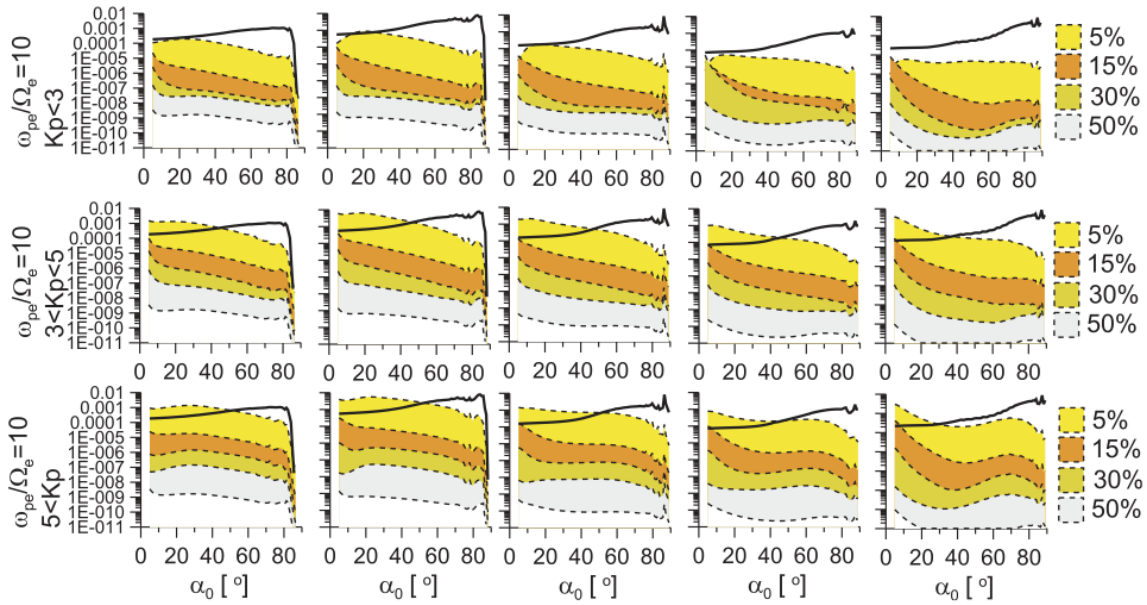


Figure 1: The effect of the amplitude of the waves on the diffusion coefficients. The coloured bands represent the contribution of the top 5%, followed by groups containing the next 15% and 30% of the amplitude distributions. (Figure adapted from *Artemyev et al. (2012)*)

significant and important for the evaluation of the diffusion coefficients. As was shown in the common paper by participants of the project, LPC2E and UCB 20% of most intense waves can ensure up to 95% of the total angular diffusion of the energetic particles.

This statement is illustrated by Figure 1 (adapted from Figure 3 from *Artemyev et al. (2012)*). All observed waves for the L-shells 4-5 were separated to groups, first of all 5% of most intense, then 15% of most intense from remaining and so on. For each group the angular diffusion quasilinear coefficients were evaluated separately, and then the relative input of each wave group to total diffusion was estimated. Two upper bands in the Figure correspond to the two groups of waves containing amplitudes in the top 5% of observations and the next 15% of most intense waves.

On the basis of this we introduced a special criteria of the selection of waves based on their amplitude, that will be discussed for each group of waves separately later.

Spacecraft	Operational dates		Total duration	Apogee/Perigee km	Inclination deg
	Start	End			
DE-1	03.08.1981	23.06.1984	3 yr 1 mo	568/23289	89.9
Polar	27.02.1996	16.06.1997	1 yr 2 mo	185/50551	85.9
CRRES	25.07.1990	04.12.1991	1 yr 5 mo	350/33580	18
THEMIS	18.02.2007	present	3s/c * 8 yr	470/87330	16
Cluster	01.02.2001	present	4s/c * 14 yr	17200/120500	90.7

Table 1: Spacecraft missions to be used in the WP4

Spacecraft	Name	L-shell	MLat	Frequency	Number of channels
DE-1	PWI	2 - 8	-20 - 20	$1.78 - 4.1 \cdot 10^5$	128
Polar	PWI	2 - 8	-20 - 20	$24 - 1.25 \cdot 10^4$	96
CRRES	PWE	0.95 - 7	-15 - 15	$104 - 4 \cdot 10^5$	128
THEMIS	SGM	2 - 8	-20 - 20	1.26 - 5994	6
Cluster	STAFF-SA	3 - 5	-20 - 20	$8.8 - 3.56 \cdot 10^3$	27

Table 2: Instrument to be used in the study

3 Description of data to be used in the WP4

The data from the following spacecraft missions and instruments will be used Cluster (*Escoubet et al., 1997*) STAFF-SA (*Cornilleau-Wehrlin et al., 1997*); DE-1 PWI (*Gurnett et al., 1995*); CRRES PWE (*Anderson et al., 1992*); POLAR PWI (*Gurnett et al., 1995*); THEMIS SGM (*Bonnell et al., 2008*). Tables 1 and 2 summarise the list of spacecraft missions used in WP4. The wave data from Cluster, DE-1, CRRES, POLAR, and THEMIS are available in LPC2E prior to the start of the PROGRESS project.

As the example the coverage by the Cluster mission of the regions where low band chorus and hiss emissions are observed is shown in Figure 2. This figure shows a histogram of the number of spectra made by the Cluster STAFF-SA instrument as a function of L-shell and MLT depending upon the level of geomagnetic activity. It can clearly be seen that for priors of low geomagnetic activity ($K_p < 3$) there is a vast amount of data that is available to be analysed, comprehensively covering all MLT and L-shells in the range 3-7. As geomagnetic activity increases, the data coverage reduces considerably due to the rarity of such periods.

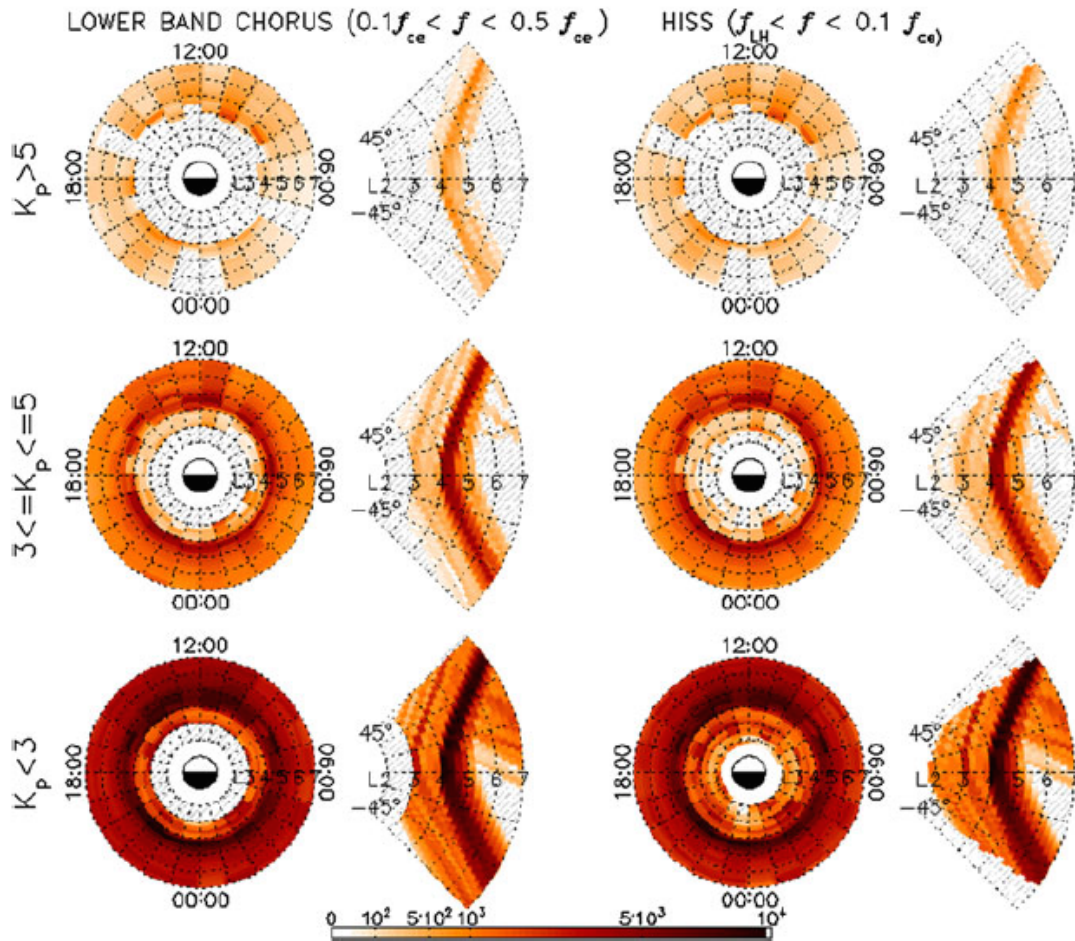


Figure 2: Data Coverage (number of spectra recorded) for the Cluster STAFF-SA measurements for the low band chorus frequency range (left panels) and for the hiss frequency range as a function L-shell and Magnetic Local Time. (Figure from *Agapitov et al. (2013)*)

4 Statistical occurrence of chorus, hiss and EMW emissions

4.1 Distribution of lower band chorus

Chorus waves are electromagnetic waves that are observed in two frequency bands above and below the half electron gyrofrequency (lower and upper band chorus). It has been demonstrated that these waves interact strongly with the electron population of the radiation belts leading to particle acceleration and losses, due to pitch angle scattering into the loss cone (e.g. *Shprits et al.*, 2008).

In this study we concentrate on the statistics of lower band chorus emissions. Upper band chorus emissions are left outside the scope of the present study since their frequency range is too high to enable a comprehensive study utilising data from all of the above listed missions. In addition, their intensity and their effect on the dynamics of high energy electrons is significantly lower than that of lower band chorus (*Meredith et al.*, 2001; *Haque et al.*, 2010). However, their effect on the lower energy electrons should not be underestimated.

The average intensity of the lower and upper band chorus obtained for the whole period of Double Star-TC1 operations are shown in Figure 3. This figure is adapted from a joint publication authored by two of the PROGRESS beneficiaries, USFD and LPC2E (*Aryan et al.*, 2014). As mentioned above, this report will concentrate on the occurrence of lower band chorus emissions. It can be seen from this figure that high amplitude lower band chorus waves during the periods of high ($AE > 300$ nT) and medium ($100 < AE < 300$) geomagnetic activity in the equatorial region are observed in the sector that extends from the early morning ($MLT \approx 3$) to the around midday ($MLT \approx 13$). During the quiet periods equatorial lower band chorus are observed roughly in the same region, but their intensity is significantly lower. At midlatitudes during the periods of medium and high activity high intensity low band chorus are observed in the sector ($MLT \approx 6$) to the around midday ($MLT \approx 13$). Again during the quiet periods intensity of midlatitude

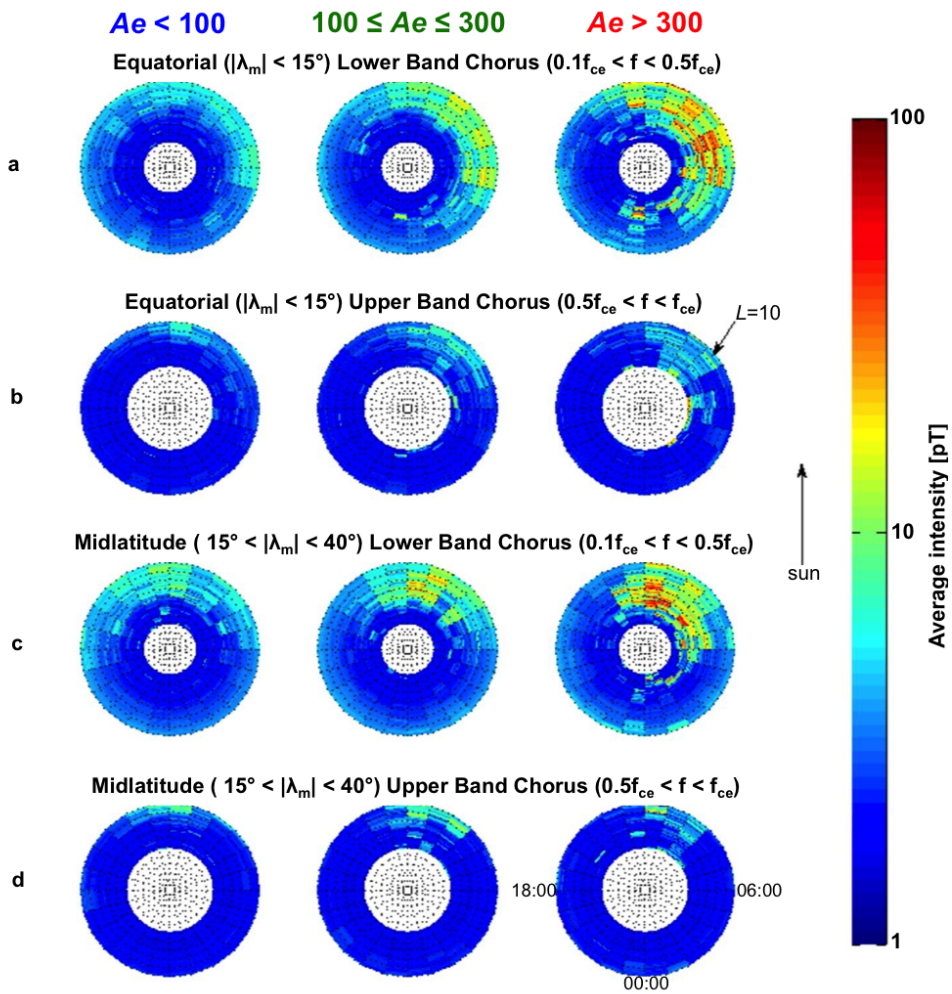


Figure 3: The distribution of lower and upper band chorus waves observed by the Double Star TC-1 satellite.

chorus is significantly lower in comparison to the more active periods. However their occurrence extends further towards the evening sector (up to about $MLT \approx 18$). Intensity of the upper band chorus waves are significantly lower in comparison to lower band chorus and they are mainly confined to the much narrower sector ($MLT \approx 9$) to the around midday ($MLT \approx 13$), for all level of geomagnetic activity.

Figure 4 shows the average amplitude distribution of lower band chorus waves as a function of magnetic local time (MLT), L-Shell, magnetic latitude (λ), and geomagnetic activity (defined by the value of Kp) based in observations by the STAFF Spectral Analyser on Cluster 4 during the period 2001-2010. The panels in the top row of Figure 4 show wave amplitude distributions for observations in the vicinity of the magnetic equator ($|\lambda| < 15^\circ$). For geomagnetically quiet periods for which $Kp < 3$ (left hand plot) it is clearly seen that the most intense waves are observed in the morning sector, in the range $04 < MLT < 14$ and $6 < L\text{-Shells} < 10$ and having amplitudes typically $B_w > 40$ pT. On the dusk sector ($14 < MLT < 19$) the wave amplitude is lower than that observed in the morning sector by almost an order of magnitude whilst the lowest intensity waves ($B_w \sim 5$ pT) are observed between MLT of 19 and 04. This distribution is essentially similar to that observed during periods of moderate to high geomagnetic activity (right hand panel) in which the strongest wave intensities are observed in the morning sector bounded in the region $9 < MLT < 12$ and $6 < L\text{ shell} < 10$ and complements the results from Double Star (Figure 3).

Meredith et al. (2012) analysed the wave measurements from a number of satellite missions (DE1, CRRES, Cluster 1, Double Star-TC1 (for only one year of operation) and THEMIS. Figures 4 and 5 from *Meredith et al.* (2012) generally correspond to the Figures 3 and Figure 4. The difference is that combined satellite model for the equatorial chorus shows more extended region of both lower and upper band chorus. For quite and medium activity ($AE < 300$ nT) the higher lower band chorus are observed in the sector from about midnight to $MLT \approx 13$. For more active periods ($AE > 300$) this region extends even

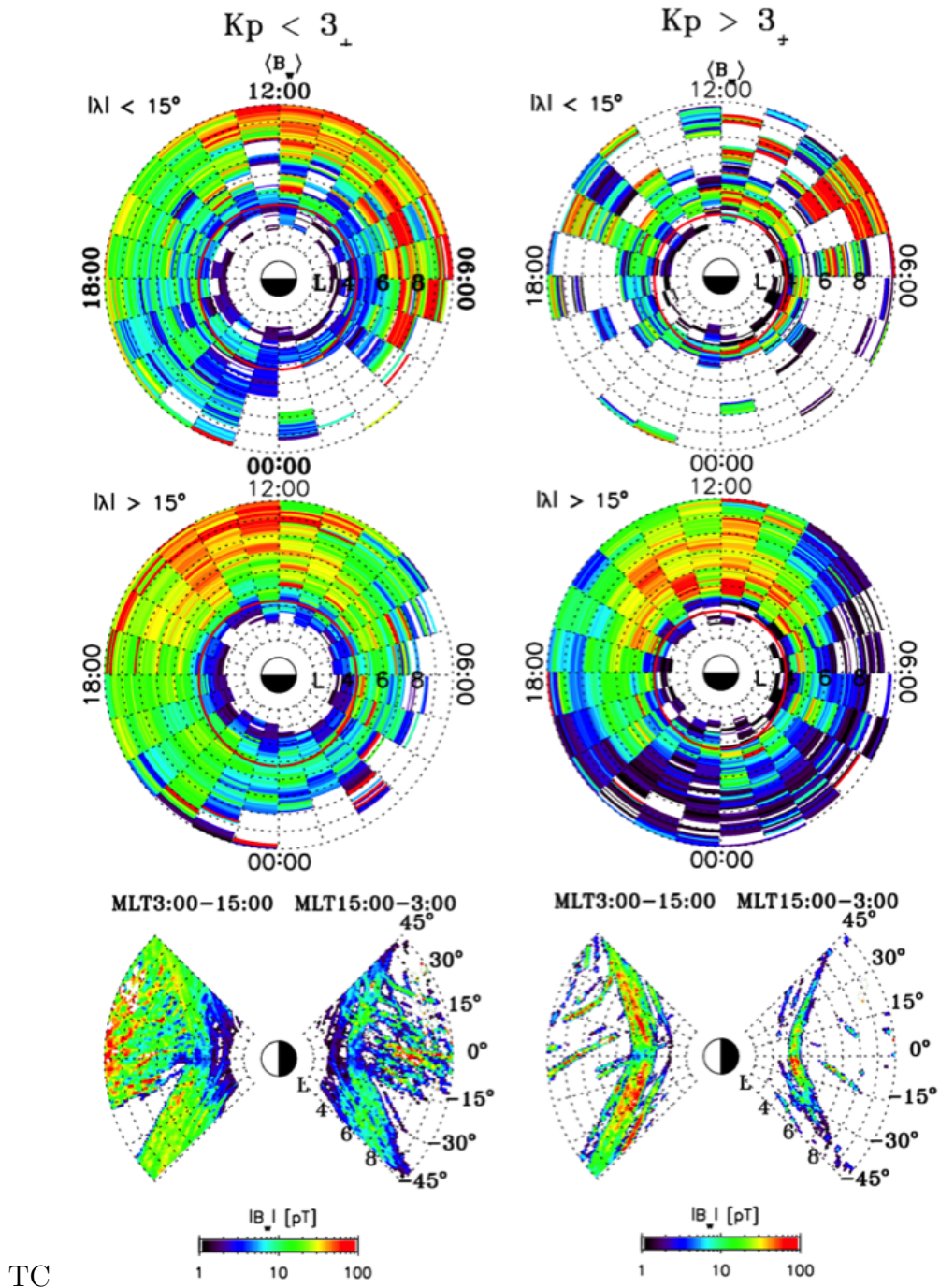


Figure 4: The averaged intensities of Chorus wave for quiet geomagnetic conditions during which $K_p \leq 3$ (left hand column) and $K_p > 3$ (right hand column). The top two rows shows the MLT-Lshell distributions for observations in the vicinity of the magnetic equator ($|\lambda| < 15^\circ$) higher latitude emissions ($|\lambda| > 15^\circ$) in the top and middle rows respectively. The bottom row shows the latitude distributions integrated in the MLT ranges 03-15 (morning sector) and 15-03 (night sector). (Taken from *Agapitov et al. (2013)*)

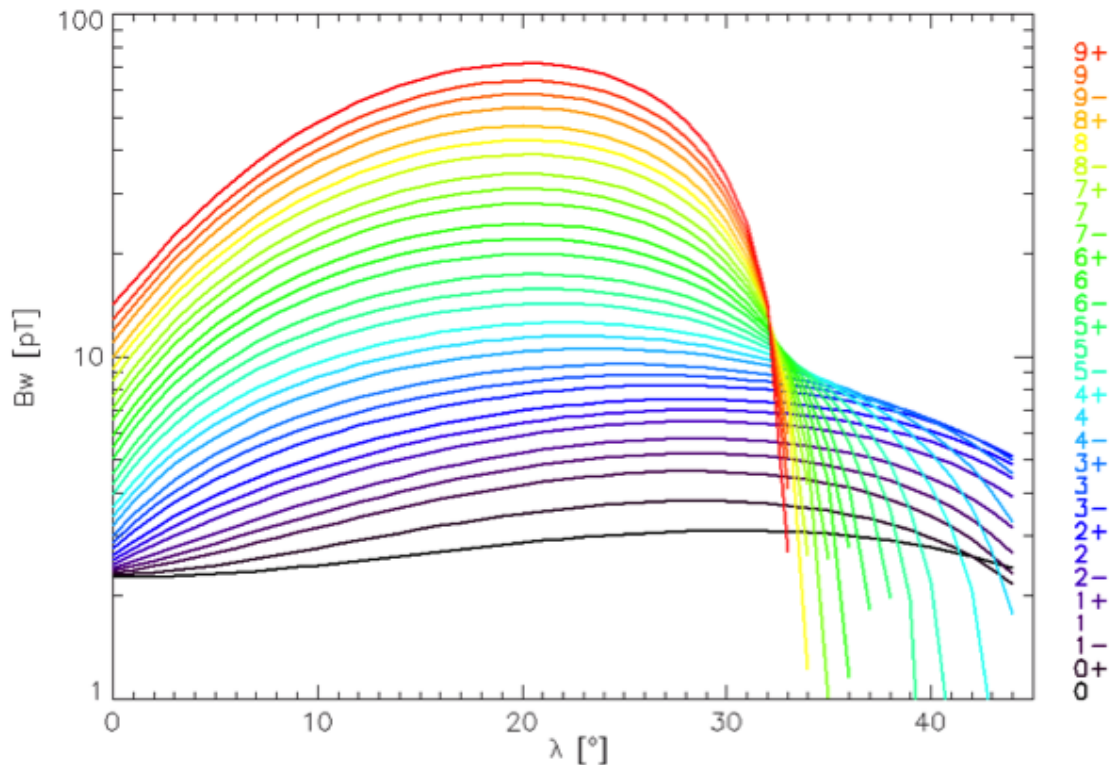


Figure 5: The variation of the amplitude of lower band chorus emissions with magnetic latitude for various levels of the geomagnetic index Kp.(Based on the results of Agapitov et al. (2015))

further starting from about $MLT \approx 13$.

A statistical study of the variation in amplitude of lower band chorus with magnetic latitude has been performed by our collaborator at UCB together with the beneficiary LPC2E using a large date set of VLF waves measured by STAFF-SA instrument on board of Cluster 4 spacecraft between February 2001 and December 2010 over a wide domain confined to $|\lambda| < 45^\circ$ and $4 \leq L \leq 7$. Figure 5 shows the results of modelling this variation using 3rd degree polynomials. Hence, knowing the equatorial amplitude of the waves we can easily compute the amplitudes at higher magnetic latitudes.

Therefore, the ERR will be applied to the equatorial region only and the amplitudes at higher latitudes will be calculated using this statistical dependence.

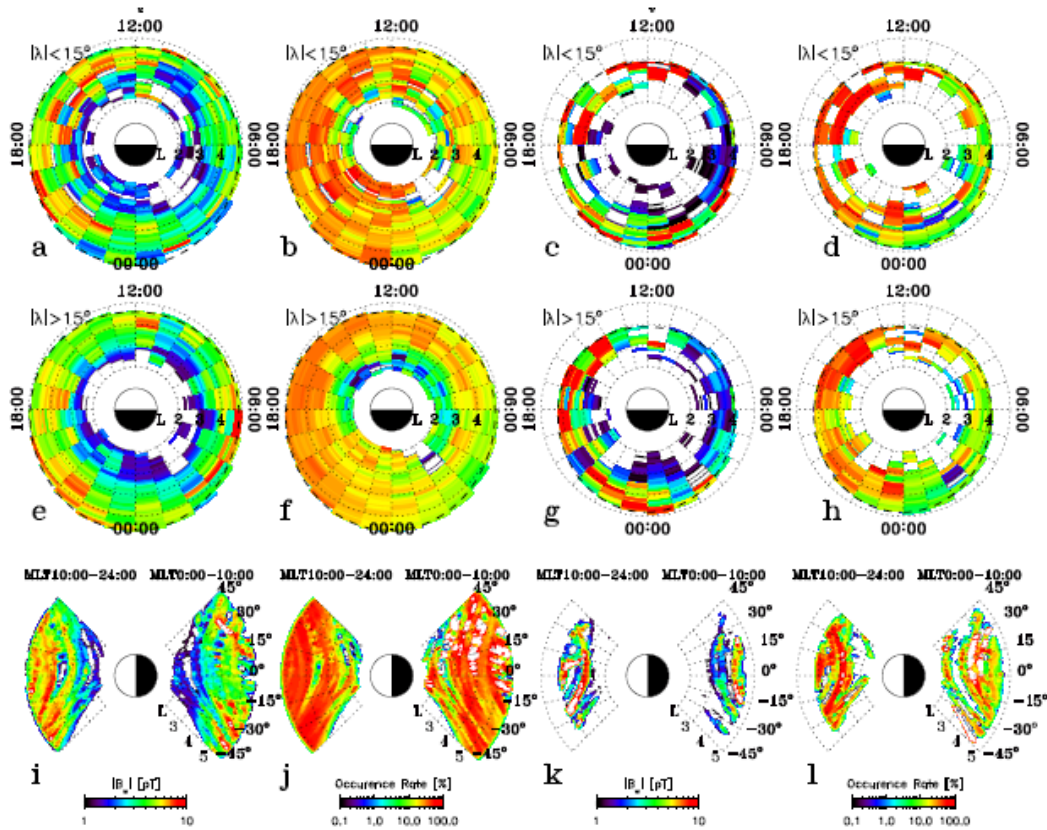


Figure 6: The spatial distribution of the observations of hiss emissions by Cluster. The averaged intensities (first and third columns) and occurrence (second and fourth columns) of Hiss waves observed by the Cluster satellites. (Taken from *Agapitov et al. (2013)*).

4.2 Distribution of Hiss

Plasmaspheric hiss emissions are electromagnetic waves usually observed in the frequency range 100Hz-several kHz, within high density regions e.g. plasmasphere and plumes. Hiss waves are responsible for the pitch angle scattering and hence loss of electrons from the radiation belts over a wide range of energies and L-shells (*Meredith et al., 2006; Summers et al., 2007*).

The spatial distribution of the occurrence of hiss waves is shown in Figure 6. The top two rows show the MLT-L-shell distributions, with the first and third column indicating the averaged intensities of waves and the second and fourth columns showing their occurrence. These emissions are typically observed at all MLT and L-shells and are increase

in intensity with increasing geomagnetic activity. The bottom row shows the amplitude and occurrence variation as a function of magnetic latitude, integrated over the morning and afternoon sectors.

Within the project, we will consider only hiss recorded within the vicinity of the equator. In order for our results to be applicable to higher latitudes, the partner LPC2E and collaborators at UCB will develop a statistical relationship between the amplitude of equatorial hiss and that observed at higher latitudes, similar to that developed for chorus (see Figure 5).

4.3 Distribution of Equatorial Magnetosonic Waves (EMW)

EMW are electromagnetic waves observed between the proton gyrofrequency and the Lower Hybrid frequency. They possess a discrete spectrum, with emissions at harmonic frequencies of the proton gyrofrequency, propagate almost perpendicular to the external magnetic field direction and are spatially confined to within a few degrees of the geomagnetic equator. These emissions have been shown to accelerate radiation belt electrons to high energies (*Horne et al.*, 2007).

Figure 7 (from (*Mourenas et al.*, 2013)) shows the MLT-L-shell distribution of EMW observed by the Cluster 4 satellite for all levels of geomagnetic activity and magnetic latitude. The strongest emissions are observed in the afternoon MLT sector, typically in the range $11 < \text{MLT} < 17$ and L shells in the range 4-5.

5 Chosen locations for Chorus, Hiss and EMW emissions

The statistical study, presented above, that has been performed by the partner CNRS-LPC2E, together with one of our unfunded collaborators at the University of California, Berkeley, and participation of USFD has demonstrated the statistical dependence between the mean amplitudes of equatorial chorus, hiss, and EMW observations and their

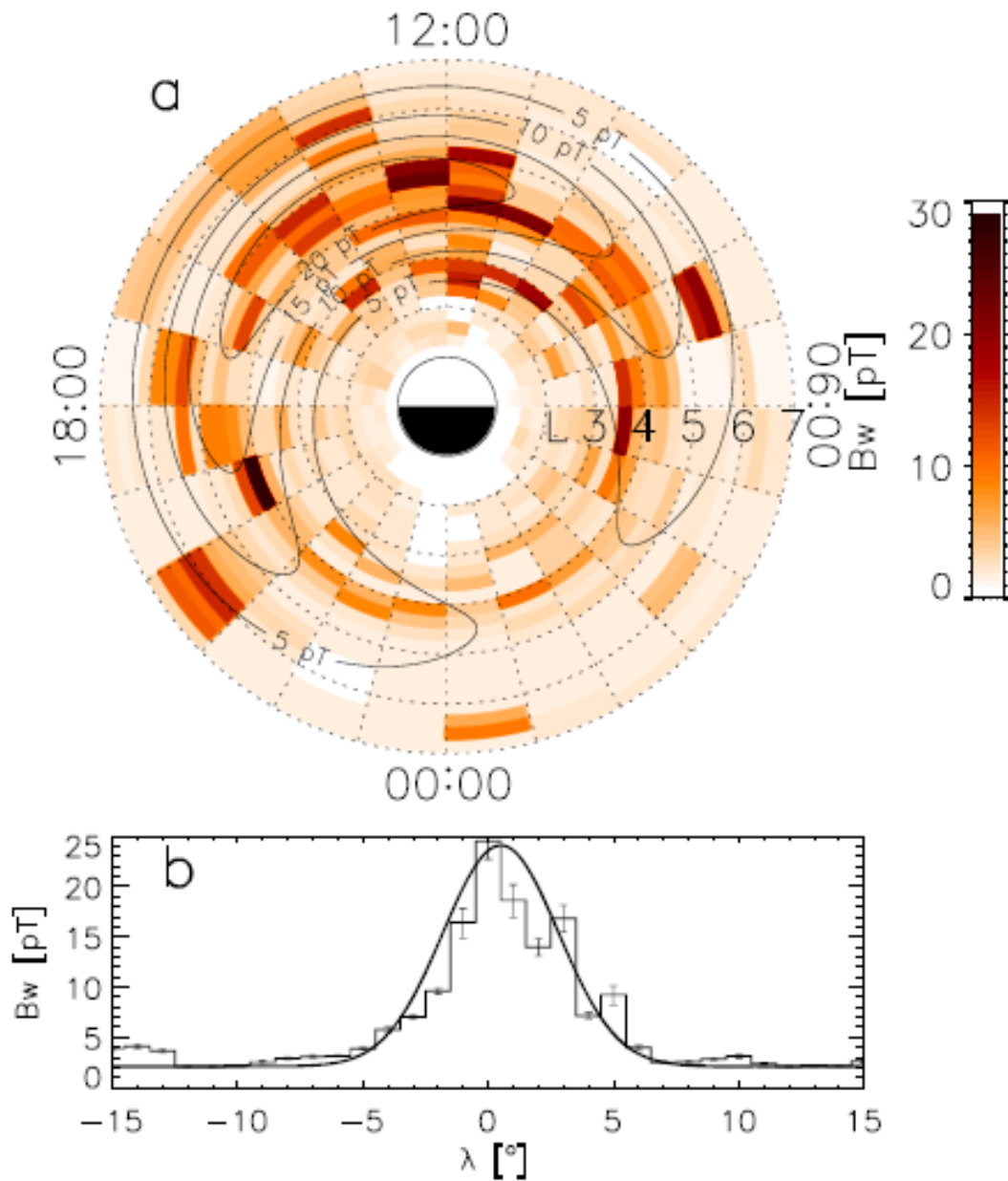


Figure 7: The averaged intensities of Magnetosonic waves for all levels of geomagnetic activity and magnetic latitudes. (Taken from (*Mourenas et al.*, 2013)).

dependence on geomagnetic activity and magnetic latitude. It was shown that the intensity of these waves varies in different regions of the magnetosphere. This information is used within this section to identify the extent of locations/regions within the magnetosphere to be used as the basis for the ERR analysis for the various wave emissions. ERR (see Appendix 1 for a description) is a systems based analysis methodology to determine which 'system input parameters' (e.g. solar wind density, pressure, magnetic field, and/or geomagnetic activity level such as Kp, Dst, or AE) most strongly influence the 'system output parameters', in this case the amplitude of the observed waves.

As has already been pointed out, in order to successfully use the ERR methodology a large number (1000 or at least 800-900) independent 'output' data points are required. For the purposes of this study, independent output points correspond to the magnetic wave intensity averaged over a particular satellite track as it passes through one spatial bin defined as the volume in the equatorial region such that the radial size corresponds to 1 L-shell and an azimuthal width of 1 hour MLT. The boundaries of the bins correspond to integer values of L in the radial direction and integer values of MLT azimuthally. Thus, in order to obtain the required high number of points required by ERR we need to define a spatial grid in MLT/L-shell space for which a number of the resulting spatial regions are traversed by about a thousand satellite tracks. However, it is also important to keep any spatial structure related to the occurrence of waves, implying the use of small spatial regions. Thus there is a trade off between these two constraints.

5.1 Chorus

The histogram of the Cluster 4 orbits during which chorus emission with amplitudes greater than 5 pT were observed during the ten year period (years 2001-2010) as a function of MLT is shown in Figure 8. This histogram shows data from a single Cluster spacecraft. As all four Cluster satellites have exactly the same wave complex and very close trajectories, to estimated the number of chorus events observed by the whole fleet of 4 Cluster satellites the values in the histogram should be multiplied by 4. The Cluster

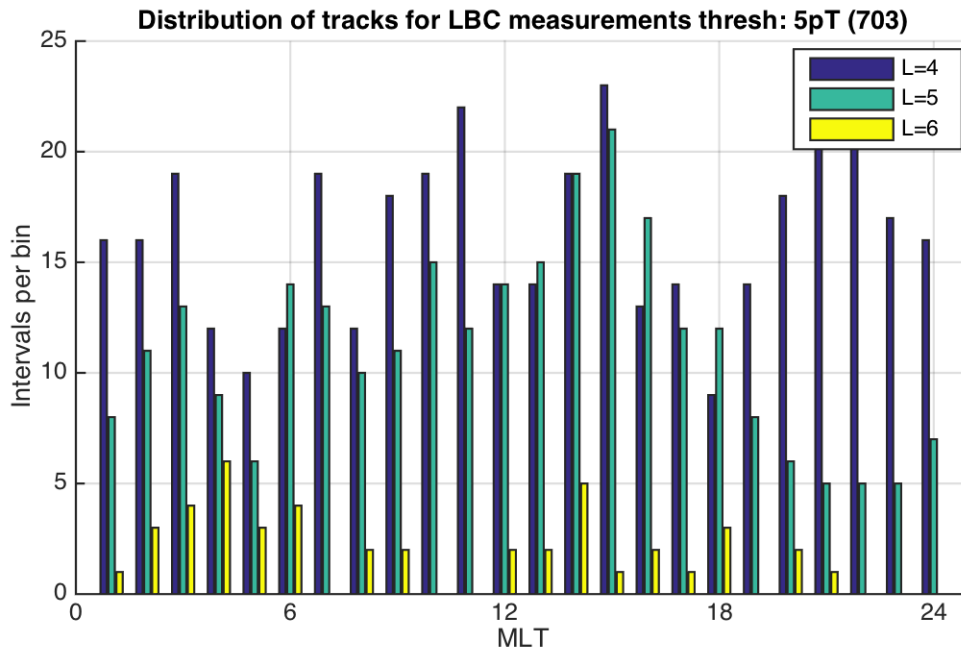


Figure 8: Distribution of satellite tracks as a function of MLT and L-shell for Lower Band Chorus emissions observed by Cluster 4 during the time period February 2001 to November 2010. The MLT bin size is 1 hour centred upon the time indicated. The L-shell bin size is 1. Only observations of waves with an amplitude greater than 5pT were used in the selection of satellite tracks.

project has over 15 years of measurements but the data presented in Figure 8 are result of only 10 years of operation. A straightforward estimate of the overall number of orbits where chorus were registered requires a further multiplication by a factor 1.5. Therefore, the values in Figure 8 should be multiplied by factor 6 in order to obtain a realistic estimate of the possible number events from the Cluster mission.

Figure 9 shows the results from a similar analysis using data from 2010 for the THEMIS A spacecraft using a similar format to the Cluster data and the same threshold (5 pT) shown in Figure 8. Since THEMIS had a more equatorial orbit, data are available for a wider range of L-shells. In order to convert these numbers into an estimate of the total

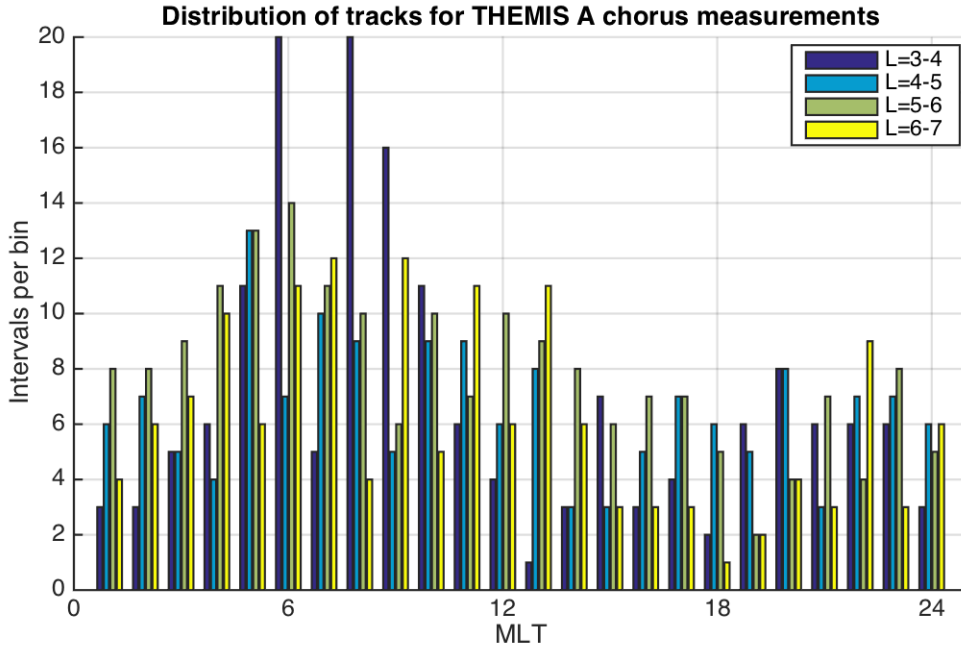


Figure 9: Distribution of satellite tracks as a function of MLT and L-shell for Lower Band Chorus emissions observed by the THEMIS A spacecraft in 2010. Only observations of waves with an amplitude greater than 5pT were used in the selection of satellite tracks.

number of events that may be expected from use of the whole THEMIS dataset a factor 21 should be used (3 satellites in relevant orbits, 7 years of operation).

However to make a very conservative estimate the factor 4 instead of 6 is used for Cluster data and factor 10 instead of 21 for THEMIS. The study of the resulting conservative estimate of data sets from Cluster and THEMIS missions lead to the following definition of spatial regions (locations) for performing ERR analysis for chorus. For local time range from 04 to 16 the azimuthal width of single "bin" is 4 hours MLT. The MLT range 16-04, where we expect lower Chorus occurrence the bin's width is 6 hours MLT. The radial size is $2L$ (ranges $L = 3$ to $L < 5$ and from $L = 5$ to $L < 7$). Table 3 lists the number of expected data points for the chosen set of locations ("bins"). The range

MLT	L-shell	
	3<L<5	5<L<7
04-08	1162	1018
08-12	952	894
12-16	888	970
16-22	1150	665
22-04	994	1118

Table 3: Estimated number of Chorus events available using data from the Cluster and THEMIS satellites in various spatial locations.

of numbers except one location (16-22 MLT, 5-7 L) is from 888 to 1162. It is possible to perform a reliable ERR analysis for a data set of these sizes. The single remaining location (6-22 MLT, 5-7 L) has an estimate of only 665 points, that is not ideal for ERR. However taking into account that the estimate is very conservative and data sets from the remaining four missions overall number of points in this bin should be sufficient.

5.2 Hiss

The analysis process described above for chorus waves was applied to Cluster 4 and THEMIS A observations of hiss emissions with exactly the same threshold 5 pT. Figures 10 and 11 show the distributions of the tracks of Cluster 4 and THEMIS A in MLT and L-shell respectively.

The estimate of number of data that are available for hiss ERR analysis has been carried out for hiss in the similar fashion as for chorus waves, described above. It was aimed at the conservative estimate and employed coefficients 4 and 10 for Cluster and THEMIS respectively. The analysis of the resulting number data sets from these missions lead to the following definition of spatial regions (locations) for performing ERR analysis for hiss data. For local time range from 04 to 22 the azimuthal width of single "bin" is 4 hours MLT. For the MLT range 22-04, the bin's width was chosen as 6 hours MLT to ensure the sufficient number of data points. The radial ranges for hiss were the same as for chorus (ranges $L = 3$ to $L < 5$ and from $L = 5$ to $L < 7$). Table 3 lists the number

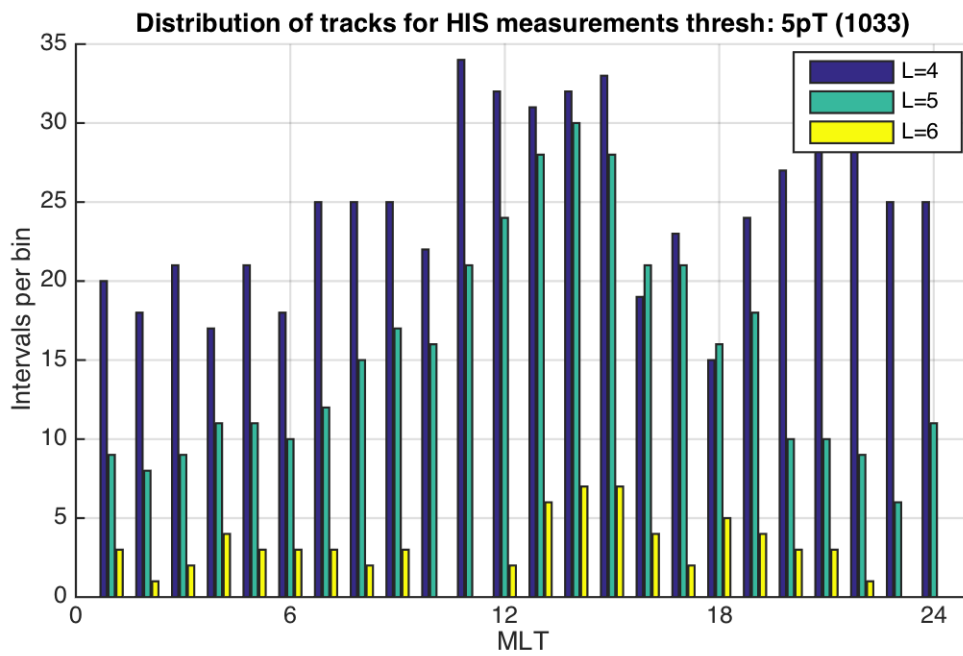


Figure 10: Distribution of satellite tracks as a function of MLT and L-shell for Hiss emissions observed by Cluster 4 during the time period February 2001 to November 2010. The former is the same as that used in Figure 8. An amplitude threshold of 5pT was used in the selection of satellite tracks.

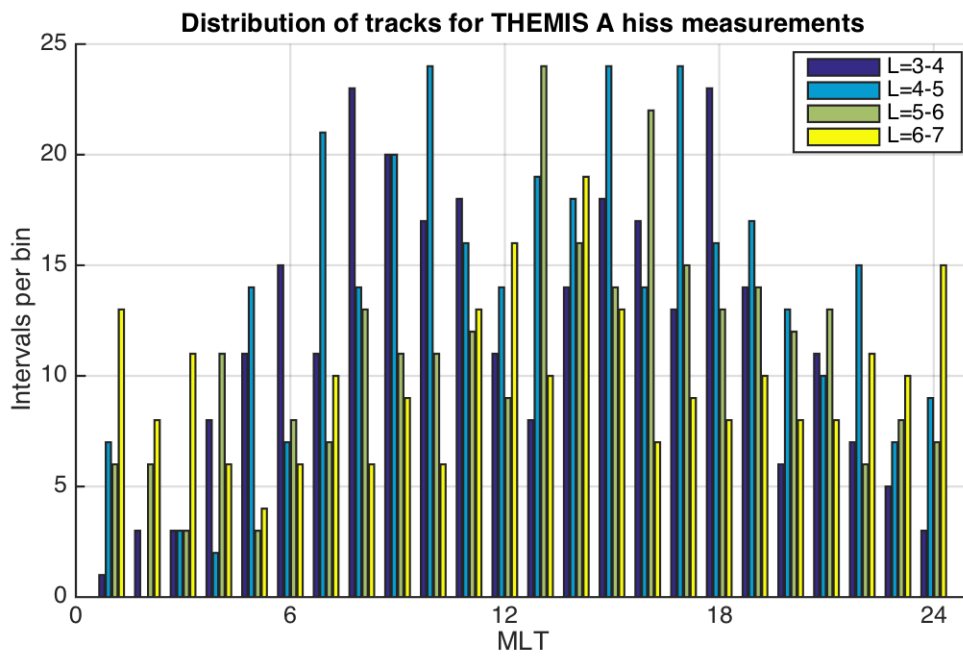


Figure 11: Distribution of satellite tracks as a function of MLT and L-shell for hiss emissions observed by THEMIS A. An amplitude threshold of 5pT was used in the selection of satellite tracks.

MLT	L-shell	
	3<L<5	5<L<7
22-04	1014	1108
04-08	1516	806
08-12	2220	1787
12-16	1780	1774
16-20	1616	1206
20-24	1118	940

Table 4: Estimated number of hiss events available using data from the Cluster and THEMIS satellites in various spatial locations.

of expected hiss data points for the chosen set of locations. The range of numbers except one location is from 806 to 2220. It is possible to perform a reliable ERR analysis for a data set of these sizes. However due to our estimate being very conservative and the data from the remaining missions we expect greater actual numbers.

5.3 Equatorial Magnetosonic Waves

Finally, this analysis was applied to the occurrence of EMW emissions. Figures 12 and 13 show the distribution of the number of satellite tracks as a function of MLT and L-Shell using a bin size of 1 hour MLT and one L-Shell for satellite tracks from Cluster and THEMIS A respectively. The amplitude threshold used for the EMW emissions was 7pT for both spacecraft. The same method as for chorus and hiss that employs coefficients 4 (Cluster) and 10 (THEMIS), was applied to EMW data to provide a a very conservative estimate of the total number of events expected. Elaboration of the resulting data sets numbers leads to the following definition of spatial regions for performing ERR analysis using the EMW data. In the radial dimension the boundaries of the bins were chosen as for chorus and hiss, namely the ranges $L = 3$ to $L < 5$ and from $L = 5$ to $L < 7$. Due to the substantial difference in resulting numbers between these two ranges the MLT widths were chosen separately for each range. For the range $L = 3$ to $L < 5$ all bin widths are 4 hours MLT. For the range $L = 5$ to $L < 7$ and MLT in the range 04 to 22 the azimuthal width of single "bin" is 4 hours MLT. For the MLT range 22-04, a single bin with width

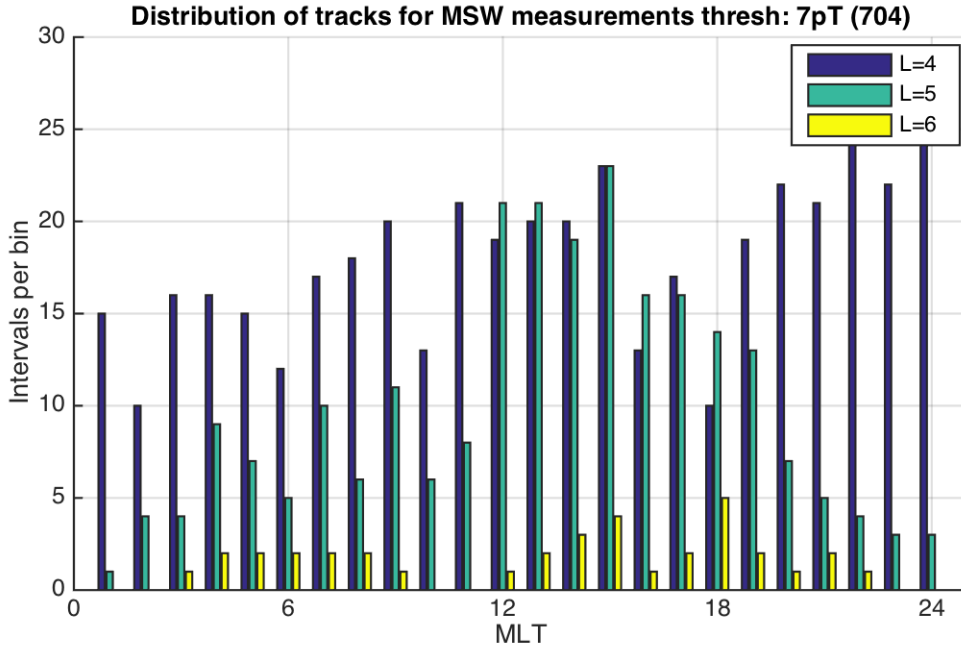


Figure 12: Distribution of satellite tracks as a function of MLT and L-shell for Equatorial Magnetosonic Waves observed by Cluster 4 during the time period February 2001 to November 2010. The former is the same as that used in Figure 8. An amplitude threshold of 7pT was used in the selection of satellite tracks.

6 hours MLT was chosen to ensure the sufficient number of data points. Table 5 lists the number of expected EMW data points for the chosen set of locations. Thus, each bin contains between 840 and 1822. Even using our conservative estimates there appears to be sufficient points to perform a reliable ERR analysis for this data set.

6 Conclusion

In this report we have presented the results of an analysis to determination the characteristics of variations in the spatial occurrence of chorus, hiss and EMW and developed the methodology to enable the definition of specific regions that contain sufficient mea-

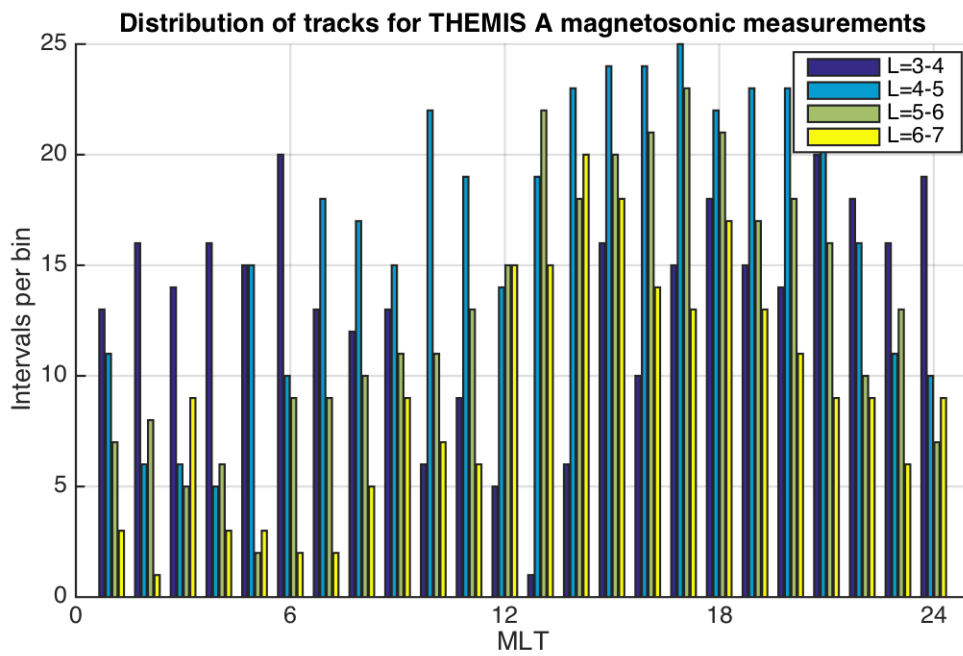


Figure 13: Distribution of satellite tracks as a function of MLT and L-shell for Equatorial Magnetosonic Waves observed by THEMIS A during 2010. The former is the same as that used in Figure 8. An amplitude threshold of 7pT was used in the selection of satellite tracks.

MLT	3<L<5
00-04	1098
04-08	1448
08-12	1322
12-16	1534
16-20	1822
20-24	1704
MLT	5<L<7
22-05	762
05-11	1152
11-15	1806
15-19	1666
19-23	840

Table 5: Estimated number of EMW events available using data from the Cluster and THEMIS satellites in various spatial locations.

surements to be subsequently used for ERR modelling.

This list of regions shown in Tables 3, 4, and 5 represents a set of locations that can be subjected to the ERR analysis. Using a conservative strategy to estimate the potential number of data points for use in the subsequent ERR analysis each spatial bin typically contains around 1000 samples. While 3 THEMIS satellites at orbits close to the equator will provide the majority of independent data points, that we expect to be sufficient for the ERR analysis, if needed the data from the four spacecraft fleet of Cluster (high inclination orbit) can be added as well as the data from the remaining missions remaining missions Polar, CRRES, DE-1.

7 Future work that utilises the results described in the deliverable 4.1.

Regions of geospace corresponding to bins that were determined in the task 4.1 will be used as guide to determine the locations for which and Error reduction Analysis will be applied to identify the parameters that govern dynamics of Chorus, hiss and EMW emissions there. At the further stage the wave models will be deduced separately for the

individual regions.

References

- Agapitov, O., A. Artemyev, V. Krasnoselskikh, Y. V. Khotyaintsev, D. Mourenas, H. Breuillard, M. Balikhin, and G. Rolland (2013), Statistics of whistler mode waves in the outer radiation belt: Cluster STAFF-SA measurements, *J. Geophys. Res. (Space Physics)*, *118*, 3407–3420, doi:10.1002/jgra.50312.
- Agapitov, O. V., A. V. Artemyev, D. Mourenas, F. S. Mozer, and V. Krasnoselskikh (2015), Empirical model of lower band chorus wave distribution in the outer radiation belt, *J. Geophys. Res. (Space Physics)*, *120*(12), 10,425–10,442, doi:10.1002/2015JA021829.
- Anderson, R. R., D. A. Gurnett, and D. L. Odem (1992), CRRES plasma wave experiment, *J. Spacecraft and Rockets*, *29*, 570–573, doi:10.2514/3.25501.
- Artemyev, A., O. Agapitov, V. Krasnoselskikh, H. Breuillard, and G. Rolland (2012), Statistical model of electron pitch angle diffusion in the outer radiation belt, *J. Geophys. Res.*, *117*, A08219, doi:10.1029/2012JA017826.
- Aryan, H., K. Yearby, M. Balikhin, O. Agapitov, V. Krasnoselskikh, and R. Boynton (2014), Statistical study of chorus wave distributions in the inner magnetosphere using *ae* and solar wind parameters, *J. Geophys. Res. (Space Physics)*, *119*, 6131–6144, doi:10.1002/2014JA019939.
- Billings, S. A., S. Chen, and M. Korenberg (1989), Identification of mimo non-linear systems using a forward-regression orthogonal estimator, *Int. J. Control*, *49*(6), 2157–2189.
- Bonnell, J. W., F. S. Mozer, G. T. Delory, A. J. Hull, R. E. Ergun, C. M. Cully, V. Angelopoulos, and P. R. Harvey (2008), The electric field instrument (EFI) for THEMIS, *Sp. Sci. Rev.*, *141*, 303–341, doi:10.1007/s11214-008-9469-2.

Cornilleau-Wehrlin, N., P. Chauveau, S. Louis, A. Meyer, J. M. Nappa, S. Perraut, L. Rezeau, P. Robert, A. Roux, C. De Villedary, Y. de Conchy, L. Friel, C. C. Harvey, D. Hubert, C. Lacombe, R. Manning, F. Wouters, F. Lefeuvre, M. Parrot, J. L. Pinçon, B. Poirier, W. Kofman, P. Louarn, and the STAFF Investigator Team (1997), The Cluster Spatio-Temporal Analysis of Field Fluctuations (STAFF) experiment, *Sp. Sci. Rev.*, *79*, 107–136.

Escoubet, C. P., R. Schmidt, and M. L. Goldstein (1997), Cluster - Science and mission overview, *Sp. Sci. Rev.*, *79*, 11–32.

Gurnett, D. A., A. M. Persoon, R. F. Randall, D. L. Odem, S. L. Remington, T. F. Averkamp, M. M. Debowler, G. B. Hospodarsky, R. L. Huff, D. L. Kirchner, M. A. Mitchell, B. T. Pham, J. R. Phillips, W. J. Schintler, P. Sheyko, and D. R. Tomash (1995), The polar plasma wave instrument, *Sp. Sci. Rev.*, *71*, 597–622.

Haque, N., M. Spasojevic, O. Santolík, and U. S. Inan (2010), Wave normal angles of magnetospheric chorus emissions observed on the Polar spacecraft, *J. Geophys. Res. (Space Physics)*, *115*, A00F07, doi:10.1029/2009JA014717.

Horne, R. B., R. M. Thorne, S. A. Glauert, N. P. Meredith, D. Pokhotelov, and O. Santolík (2007), Electron acceleration in the Van Allen radiation belts by fast magnetosonic waves, *Geophys. Res. Lett.*, *34*, L17,107, doi:10.1029/2007GL030267.

Horne, R. B., T. Kersten, S. A. Glauert, N. P. Meredith, D. Boscher, A. Sicard-Piet, R. M. Thorne, and W. Li (2013), A new diffusion matrix for whistler mode chorus waves, *J. Geophys. Res. (Space Physics)*, *118*, 6302–6318, doi:10.1002/jgra.50594.

Meredith, N. P., R. B. Horne, and R. R. Anderson (2001), Substorm dependence of chorus amplitudes: Implications for the acceleration of electrons to relativistic energies, *J. Geophys. Res.*, *106*, 13,165–13,178, doi:10.1029/2000JA900156.

- Meredith, N. P., R. B. Horne, S. A. Glauert, R. M. Thorne, D. Summers, J. M. Albert, and R. R. Anderson (2006), Energetic outer zone electron loss timescales during low geomagnetic activity, *J. Geophys. Res. (Space Physics)*, *111*, A05212, doi:10.1029/2005JA011516.
- Meredith, N. P., R. B. Horne, A. Sicard-Piet, D. Boscher, K. H. Yearby, W. Li, and R. M. Thorne (2012), Global model of lower band and upper band chorus from multiple satellite observations, *J. Geophys. Res. (Space Physics)*, *117*, doi:10.1029/2012JA017978.
- Mourenas, D., A. V. Artemyev, O. V. Agapitov, and V. Krasnoselskikh (2013), Analytical estimates of electron quasi-linear diffusion by fast magnetosonic waves, *J. Geophys. Res. (Space Physics)*, *118*, 3096–3112, doi:10.1002/jgra.50349.
- Shprits, Y. Y., D. A. Subbotin, N. P. Meredith, and S. R. Elkington (2008), Review of modeling of losses and sources of relativistic electrons in the outer radiation belt i: local acceleration and loss, *J. Atmos. Sol. Terr. Phys.*, *70*, 1694–1713, doi:10.1016/j.jastp.2008.06.014.
- Summers, D., B. Ni, and N. P. Meredith (2007), Timescales for radiation belt electron acceleration and loss due to resonant wave-particle interactions: 2. evaluation for vlf chorus, elf hiss, and electromagnetic ion cyclotron waves, *J. Geophys. Res. (Space Physics)*, *112*, A04207, doi:10.1029/2006JA011993.

A The Error Reduction Ratio methodology

The correlation function was developed to assess the causal relationship between two time series signals. However, this method cannot identify nonlinear relationships and should not be used when assessing the dependencies of a nonlinear system. This can easily be shown with the example system $y(t) = x^2(t)$, where $x(t)$ is a zero mean signal. Here, the correlation between $y(t)$ and $x(t)$ will be zero even though $x(t)$ is the input to the system. The Error Reduction Ratio (ERR) was developed for nonlinear system identification to determine the structure for Nonlinear AutoRegressive Moving Average eXogenous input (NARMAX) models. The ERR methodology has the ability to find a wide class of nonlinear terms and evaluate their relationship with system output.

The ERR methodology combines all of the past inputs and past output terms into a polynomial of a predetermined degree. The time series data of the monomials which make up the polynomial are then assembled into the matrix P

$$\mathbf{P} = \begin{bmatrix} p_1(1) & p_2(1) & \cdots & p_M(1) \\ p_1(2) & p_2(2) & \cdots & p_M(2) \\ \vdots & \vdots & & \vdots \\ p_1(N) & p_2(N) & \cdots & p_M(N) \end{bmatrix} \quad (1)$$

where $p_i(t)$ is the i^{th} monomial at time t , M is the number of monomials and N is the number of data points in the time series.

Each column of P , or monomial, is then assessed by the ERR

$$[ERR_1]_i = \frac{(\mathbf{p}_i^T \mathbf{y})^2}{(\mathbf{y}^T \mathbf{y})(\mathbf{p}_i^T \mathbf{p}_i)} \quad (2)$$

where y is the output signal of the system.

The monomial with the highest ERR is then selected as the first term.

$$h_1 = \arg[\max\{[ERR_1]_i, 1 \leq i \leq M\}] \quad (3)$$

$$\mathbf{w}_1 = \mathbf{p}_{h_1} \quad (4)$$

$$ERR_1 = [ERR_1]_{h_1} \quad (5)$$

where \mathbf{w}_1 is the first auxiliary monomial.

The monomials of P are then made orthogonal to each other so that the individual influence of each monomial can be separated. Therefore, in the second step, the remaining monomials in P are made orthogonal to \mathbf{w}_1 .

$$\mathbf{q}_i = \mathbf{p}_i - [r_{12}]_i \mathbf{w}_1 \quad (6)$$

where

$$[r_{12}]_i = \frac{\mathbf{w}_1^T \mathbf{p}_i}{\mathbf{w}_1^T \mathbf{w}_1} \quad (7)$$

The i^{th} orthogonalised monomial is then assessed by the ERR

$$[ERR_2]_i = \frac{[g_2]_i^2 \mathbf{q}_i^T \mathbf{q}_i}{\mathbf{y}^T \mathbf{y}} \quad (8)$$

where

$$[g_2]_i = \frac{\mathbf{q}_i^T \mathbf{y}}{\mathbf{q}_i^T \mathbf{q}_i} \quad (9)$$

The orthogonalised monomial with the highest ERR is then selected as the second term.

$$h_2 = \arg[\max\{[ERR_2]_i, 1 \leq i \leq M, i \neq h_1\}] \quad (10)$$

$$\mathbf{w}_2 = \mathbf{q}_{h_2} \quad (11)$$

$$ERR_2 = [ERR_2]_{h_2} \quad (12)$$

For the n^{th} step these equations will be

$$\mathbf{q}_i = \mathbf{p}_i - \sum_{j=1}^{n-1} [r_{jn}]_i \mathbf{w}_j \quad (13)$$

where

$$[r_{jn}]_i = \frac{\mathbf{w}_j^T \mathbf{p}_i}{\mathbf{w}_j^T \mathbf{w}_j} \quad (14)$$

The i^{th} orthogonalised monomial is then assessed by the ERR

$$[ERR_n]_i = \frac{[g_n]_i^2 \mathbf{q}_i^T \mathbf{q}_i}{\mathbf{y}^T \mathbf{y}} \quad (15)$$

where

$$[g_n]_i = \frac{\mathbf{q}_i^T \mathbf{y}}{\mathbf{q}_i^T \mathbf{q}_i} \quad (16)$$

The orthogonalised monomial with the highest ERR is then selected as the second term.

$$h_n = \arg[\max\{[ERR_n]_i, 1 \leq i \leq M, i \neq h_1, h_2, \dots, h_{n-1}\}] \quad (17)$$

$$\mathbf{w}_n = \mathbf{q}_{h_n} \quad (18)$$

$$ERR_n = [ERR_n]_{h_n} \quad (19)$$

As such, the ERR methodology is able determine nonlinear monomials that influence a system.